PCCP

Accepted Manuscript

ROYAL SOCIETY OF CHEMISTRY

www.rsc.org/pccp

PCCP

Paper

Localised and Delocalised Excitons in Star-like Squaraine Homo- and Heterotrimers

Received 00th January 20xx,
Accepted 00th January 20xx

DOI: 10.1039/x0xx00000x

www.rsc.org/

Harald Ceymann, Moritz Balkenhohl, Alexander Schmiedel, Marco Holzapfel and Christoph Lambert*

Exciton coupling of localised chromophore states within covalently bound superchromophores is a viable strategy to modify optical properties such as spectral broadening and red-shifting of absorption bands. These are desirable properties for e.g. organic photovolatic applications. Attaching three squaraine dyes to a central nitrogen core in a star-shaped manner leads to the formation of superchromophores that may form localised and delocalised excitons upon photoexcitation. In this work we investigated two homotrimers, two heterotrimers and a heterodimer formed by the combination of two different squaraines SQA and SQB. Due to exciton coupling the two homotrimers display a red shift of the main absorption band by about 1000 cm^{-1} compared to their monomeric reference compounds. On the other hand, the heterotrimers show a broadening of the absorption spectra with three peak maxima at the exciton manifold band. In fluorescence experiments the homotrimers display signals similar to the emission of the monomeric compounds but red shifted. However, the heterotrimers and the heterodimer show, beside emission from the delocalised lowest energy state, an additional signal that overlaps strongly with the absorption. Excitation and time-dependent emission spectra of the hetero compounds indicate that this emission stems from a localised higher energy state.This interpretation is corroborated by transient absorption measurements with fs-time resolution.

Introduction

Spectral broadening and red-shifting of absorption characteristics of organic dyes is desirable for many applications such as organic photovoltaics.[1, 2] One strategy to achieve this goal is to substitute chromophores with e.g. donors or acceptors or to enlarge the π-system. However, by applying these strategies it is difficult to predict the dye properties. Therefore, our goal is to generate new or modified optical properties by building up superchromophores from covalently linked monomeric chromophores with known optical properties. By exciton coupling of excited states[3] new optical properties are formed in these superchromophores which are to some extent better predictable. In this way a red-shift or broadening of absorption bands, enhancement of fluorescence quantum yields[4] or generation of NIR fluorescence may be possible. The latter was e.g. realised in recently studied macrocyclic squaraine dye trimers and tetramers.[3] In this contribution we combine two different squaraine dyes **SQA** and **SQB** (being the prototypical squaraines without NHAc groups) in star-like dye conjugates by attaching them to a central nitrogen atom, see Fig. 1. Squaraine dyes were used because of their superior optical properties such as intense and narrow absorption in the red to near infrared spectral region and high fluorescence quantum yields in a number of applications.[5-20] Bringing such chromophores in close proximity will give rise to exciton coupling effects and to the formation of modified excited states compared to the monomer chromophores.[21] Therefore, we synthesised two homotrimers (**$(SQA)_3N$** and **$(SQB)_3N$**) and two heterotrimers (**$(SQA)_2(SQB)N$** and **$(SQA)(SQB)_2N$**) built up from the s-shaped squaraine **SQA** and from the c-shaped squaraine **SQB**. The latter absorbs at lower energy than **SQA** because of the dicyanovinylene group attached to the squaric acid centre.[22] For comparison, we also investigated a hetero-dimer (**(SQA)(SQB)NH**).

Before we describe the optical properties of the dye conjugates being in focus of this work, we anticipate these properties by having a qualitative look at what exciton theory[23] predicts: in case of three identical chromophore branches arranged in an ideally D_3 symmetric star-like manner the transition dipoles of the three localised transitions into the excited states of the monomers interact in the superchromophore and yield a set of degenerate excited states at lower energy (E symmetry) and a single excited state at higher energy (A symmetry) than the monomer excited state (see Fig. 2). Excitation into the former set is allowed and

* *Institut für Organische Chemie, Universität Würzburg, Wilhelm Conrad Röntgen Research Center for Complex Material Systems, Center for Nanosystems Chemistry, Am Hubland, 97074 Würzburg, Germany.*
E-Mail: christoph.lambert@uni-wuerzburg.de

Electronic Supplementary Information (ESI) available: Synthetic protocols, raw data of time resolved measurements, eigenvalues and eigenvectors of exciton coupling theory. See DOI: 10.1039/x0xx00000x

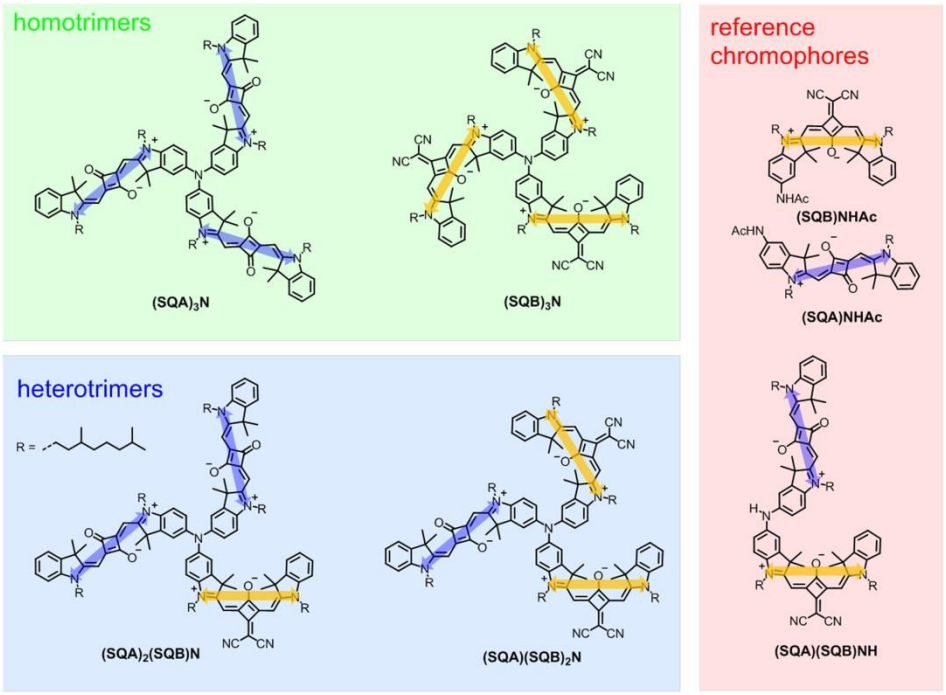

Fig. 1. Star-like squaraine homo- and heterotrimers, parent monomers and dimer along with their respective orientation of transition moments of the lowest energy localised states. The orientation of transition moments are estimated on the basis of CAMB3LYP/6-31G* computations of the monomers.

carries three times the squared transition moment ($\propto$ oscillator strength) of a monomer while the latter state is forbidden. Symmetry breaking or other structural variations will lift these constraints to some extent and will lead to the observation of all excited exciton states in a steady-state absorption spectrum. This allows extracting the exciton coupling energy *J* from the absorption spectra in a simple way as it is one third of the energy difference of the highest and lowest exciton state. In case of a heterotrimer built up from two identical and one different chromophores the situation is much more complex. Because of the reduced symmetry there are in general two different exciton coupling interactions, the one between the like and the one between the unlike chromophores. Furthermore, the exciton state energies depend on the energy difference (= $2\Delta E$) of the noninteracting excited states of the different monomer chromophores. For the special case of identical exciton coupling *J* the analytical solutions for the eigenstates are given in the supporting information (Table S11-S13). In fact, as we will show below, this is approximately the case for the squaraine dyes employed in this work. Here we refer to a qualitative description which is sufficient to describe the essential optical features of the superchromophores of interest. As can be seen from Fig. 2 exciton coupling in the heterotrimer leads to three different eigenstates in the exciton manifold. For cases where the energy difference $2\Delta E$ between the two different monomers is smaller than the coupling energy *J*, the two lower energy states are somewhat closer to each other and the upper one is farther apart, disregarding whether the two identical chromophore branches possess the higher excitation energy than the other one or vice versa. In the latter case, when the two identical chromophore branches are lower in energy, this holds true for any values of ΔE. Thus, for realistic scenarios we will observe three exciton eigenstates with different energies for heterotrimers. Furthermore, because the transition moments of the two different sorts of chromophores are in general not identical, excitation into all states will be allowed to a different degree. Presuming equal exciton coupling interactions *J*, the energy difference of the highest and lowest exciton state is larger than in case of the homotrimer. Thus, we expect that the use of different chromophores may lead to broader absorption spectra based on the broader exciton manifold.

Results

Absorption spectra. In Fig. 3 the absorption spectra of the two homotrimers, the two heterotrimers and the heterodimer are presented together with their respective monomeric reference compounds in toluene solution. From these spectra it is obvious that the two homotrimers display intense and strongly red-shifted absorption bands relative to their respective monomeric reference compounds **(SQA)NHAc** and **(SQB)NHAc** (1100 cm^{-1} for **$(SQA)_3N$** and 1000 cm^{-1} for **$(SQB)_3N$**). This is clearly caused by exciton coupling which implies delocalisation of excitation over all chromophore branches. The peak at 16100 cm^{-1} for **$(SQA)_3N$** and at 14900 cm^{-1} for **$(SQB)_3N$** indicates some structural disorder as this transition should be forbidden for a truly D_3-symmetric superchromophore. As indicated above, we used this peak to evaluate the exciton coupling energy which is given in Table 1 and which is ca. 600 cm^{-1} for both homotrimers. In contrast to the homotrimers, the heterotrimers show much more complex absorption

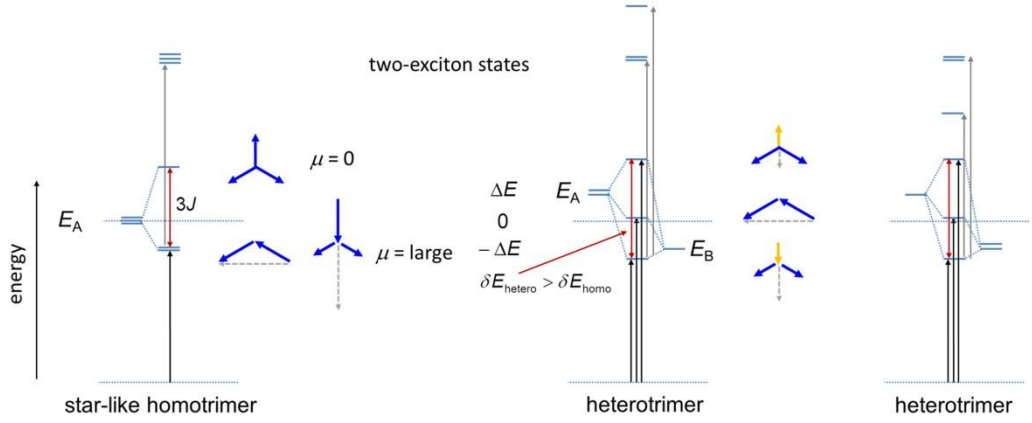

Fig. 2. Exciton eigenstates formed by exciton interaction in case of a D_3 symmetric homotrimer (left) and two heterotrimers (right). The excited state energies of the isolated monomers are given as E_A and E_B. The exciton state energies in the heterotrimers are arbitrary and depend on the relative magnitude of J and ΔE. The blue and yellow arrows indicate the phase relations of the localised transition moments. The grey dashed arrows are the resulting sum of transition moments. Allowed transition from the ground state are given as black arrows, excited state transitions as grey arrows.

Table 1. Optical steady state data of squaraine chromophores in toluene at RT.

	$\tilde{\nu}_{abs}$/cm^{-1} (ε/M^{-1} cm^{-1})	μ^2 /D^2	$\tilde{\nu}_{fl}$ /cm^{-1} [a]	ϕ_f ($\tilde{\nu}_{ex}$/cm^{-1}) [b]	$\lvert J \rvert$ /cm^{-1}
(SQA)$_3$N	14200 (352500)	313	13700	0.35 ± 0.009 (15200)	630
(SQB)$_3$N	13100 (379800)	347	12700	0.10 ± 0.002 (15300)	600
(SQA)(SQB)$_2$N	13700 (252900)	348	12600 (13600)	0.06 ± 0.007 (14900)	690[c]
(SQA)$_2$(SQB)N	13200 (136500)	346	(12700) (13700) 14900	0.04 ± 0.005 (16700)	700[c]
(SQA)(SQB)NH	13500 (204900) 15400 (199200)	239	(13200) 14900	0.12 ± 0.010 (16700)	736
(SQA)NHAc	15300 (280900)	107	15100	0.65 ± 0.035 (16100)	
(SQB)NHAc	14100 (234800)	108	13800	0.61 ± 0.030 (15600)	

[a] less intense maxima in parentheses. [b] excitation wavenumber used for measuring the fluorescence spectra and the quantum yield in parentheses. [c] average coupling.

spectra. Superchromophore **(SQA)$_2$(SQB)N** has three peak maxima in the exciton manifold band whereby the one at intermediate energy is strongest. Clearly, these peaks are associated with the three exciton states as indicated by the energy level diagram in Fig. 2. Similarly, also **(SQA)(SQB)$_2$N** shows three excitonic transitions, although the two at lower energy merge and only a shoulder is visible for the lowest energy transition.

The exciton coupling between the two different squaraines can directly be evaluated from the absorption spectrum of the dimer **(SQA)(SQB)NH** where only one coupling is present. Its spectrum shows two prominent absorptions at 13500 cm^{-1} and 15400 cm^{-1} which are distinctly shifted relative to their two reference chromophores. Exciton coupling theory predicts a splitting $\delta E_{dimer} = 2\sqrt{\Delta E^2 + J^2}$ of these bands from which J can be evaluated as 736 cm^{-1}.[24] This is ca. 20% higher than the coupling in the homotrimers. Given the crudeness of approximation, we assume equal couplings within each heterotrimer which gives (see SI) 690 and 700 cm^{-1} as "average" couplings.[25]

The squared transition moments of the exciton manifold of all superchromophores (see Table 1) reflect approximate additivity from the monomeric reference chromophores which follow the Thomas-Reiche-Kuhn sum rule[26] and show that no other transitions are involved besides those generated by exciton coupling.

Fluorescence spectra. All squaraines investigated in this work fluoresce significantly in toluene solution (Fig. 4). The monomeric reference compounds **(SQA)NHAc** and **(SQB)NHAc** show fluorescence with little Stokes shift and high quantum yield of ca. 60% (see Table 1). As expected the fluorescence displays mirror image to the absorption band. This is not the case for the homotrimers which display fluorescence signals with the shape of a monomer fluorescence but shifted to lower energies. This proves fluorescence to be emitted from the lowest exciton state only. However, the heterodimer and the heterotrimers behave quite differently. When exited at the high energy side of the exciton manifold they show complex fluorescence spectra that overlap strongly with the absorption spectra of the exciton manifold. For **(SQA)(SQB)$_2$N** the fluorescence signal shows – besides the typical monomer-shaped fluorescence at 12600 cm^{-1} – a weaker signal at 13600 cm^{-1}. For **(SQA)$_2$(SQB)N** it is the other way round: a strong monomer-shaped fluorescence is observed at 14900 cm^{-1} (together with a vibronic peak at 13700 cm^{-1}) and a second much weaker signal at 12700 cm^{-1} which stems from the lowest energy exciton state. Also noteworthy is the generally much weaker fluorescence quantum yield of the superchromophores than of the reference monomers which may be understood in terms of the energy gap rule.

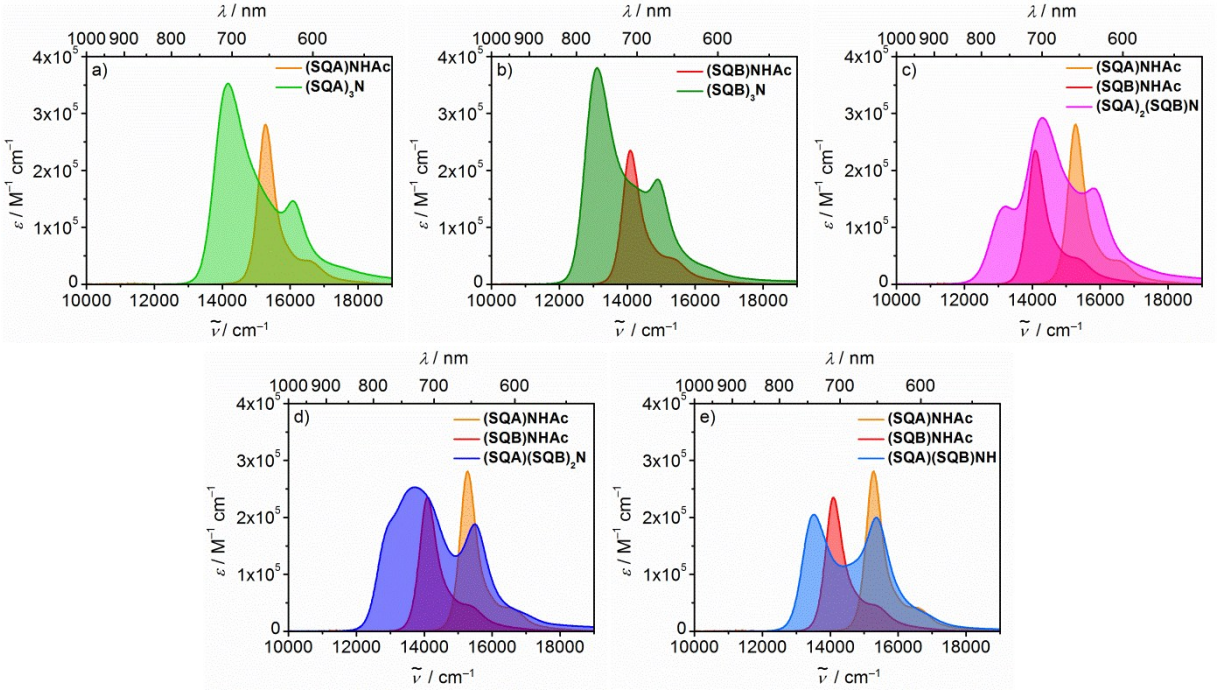

Fig. 3. Absorption spectra of superchromophore squaraines in toluene at RT. For comparison, the respective monomer spectra are also plotted.

For bringing light into this somewhat unusual behaviour of the heterochromophores we measured excitation spectra at different emission wavenumbers of the three heterochromophores. For the heterodimer **(SQA)(SQB)NH** the excitation spectrum measured at 13200 cm^{-1} emission (black solid line) looks very similar to the absorption spectrum. However, the lowest energy peak has a somewhat lower intensity which might be caused by an improper correction of the excitation monochromator at this very long wavelength region. However, the excitation spectrum at 14900 cm^{-1} (solid white line) which refers to the peak maximum of the fluorescence does not follow the absorption spectrum in this wavenumber region. Likewise, the excitation spectra of the heterotrimers measured at the wavenumber of the lowest emission peak are similar to the respective absorption spectra and those spectra measured at the wavenumber of the highest energy fluorescence peak show strong deviations. The latter observation points towards the presence of a second species that displays a different absorption spectrum.

Using TCSPC we measured the fluorescence lifetime of all squaraine dyes (see Table 2). The principal component of the NHAc substituted monomers have a lifetime of ca. 2 and ca. 3 ns and are very similar to the ones of the unsubstituted monomers SQA and SQB but the homotrimers' longest lifetime deviates significantly (1.56 ns for **$(SQA)_3N$** and 0.81 ns for **$(SQB)_3N$**). Because of the complexity of the emission spectra of the heterochromophores we measured time-dependent fluorescence spectra using TCSPC. Contour plots of these spectra are given in Fig. 4 and decay associated spectra (DAS, parallel model) from a global fit are given in the SI (Fig. S10 to Fig. S14). In all cases four components were necessary to fit the emission map adequately. The decay times associated with the DAS are collected in Table 2. Qualitatively, in all cases the lifetimes at higher emission wavenumber are on the order of 1-3 ns whereas the lifetimes at lower wavenumber are on the order of 0.1-0.5 ns. Thus, it is clear that the fluorescence of the heterochromophores stems from at least two different states where the higher energy state possesses the longer lifetime. Taking a closer look, the principal component at higher wavenumber of the emission spectrum of **$(SQA)(SQB)_2N$** (τ = 3.2 ns) has a very similar lifetime to **(SQB)NHAc** (τ = 3.0 ns), the one of **$(SQA)_2(SQB)N$** (τ = 1.7 ns) and of **(SQA)(SQB)NH** (τ = 1.9 ns) to **(SQA)NHAc** (τ = 1.9 ns). Together with the spectral similarity of these components with the respective emission spectra of the monomers we assume that the emission stems from states/species that are very similar to pure monomer states.

Time resolved spectroscopy with fs-resolution. From the steady state spectroscopy and the TCSPC measurements we conclude that in the heterochromophores a second species/state is present in solution which is deactivated by fluorescence at high energy. In order to shed light on the photoinduced dynamics of the superchromophore we performed time resolved pump-probe spectroscopy with fs-time resolution, that is, fluorescence upconversion (FLUC) and transient absorption (TA) spectroscopy.

Because of experimental limitations (small Stokes shift of fluorescence near the gate wavenumber), the fs-upconversion measurements were performed by excitation of the exciton manifold at higher wavenumber. The time resolution is on the order of ca 300 fs which is mainly caused by the wavelength dispersion of the solvent and the necessity to use a set of filters to supress stray light. The measurements were done at parallel, perpendicular and magic angle polarisation of pump and gate pulse (see Fig. S15 and S16). From these

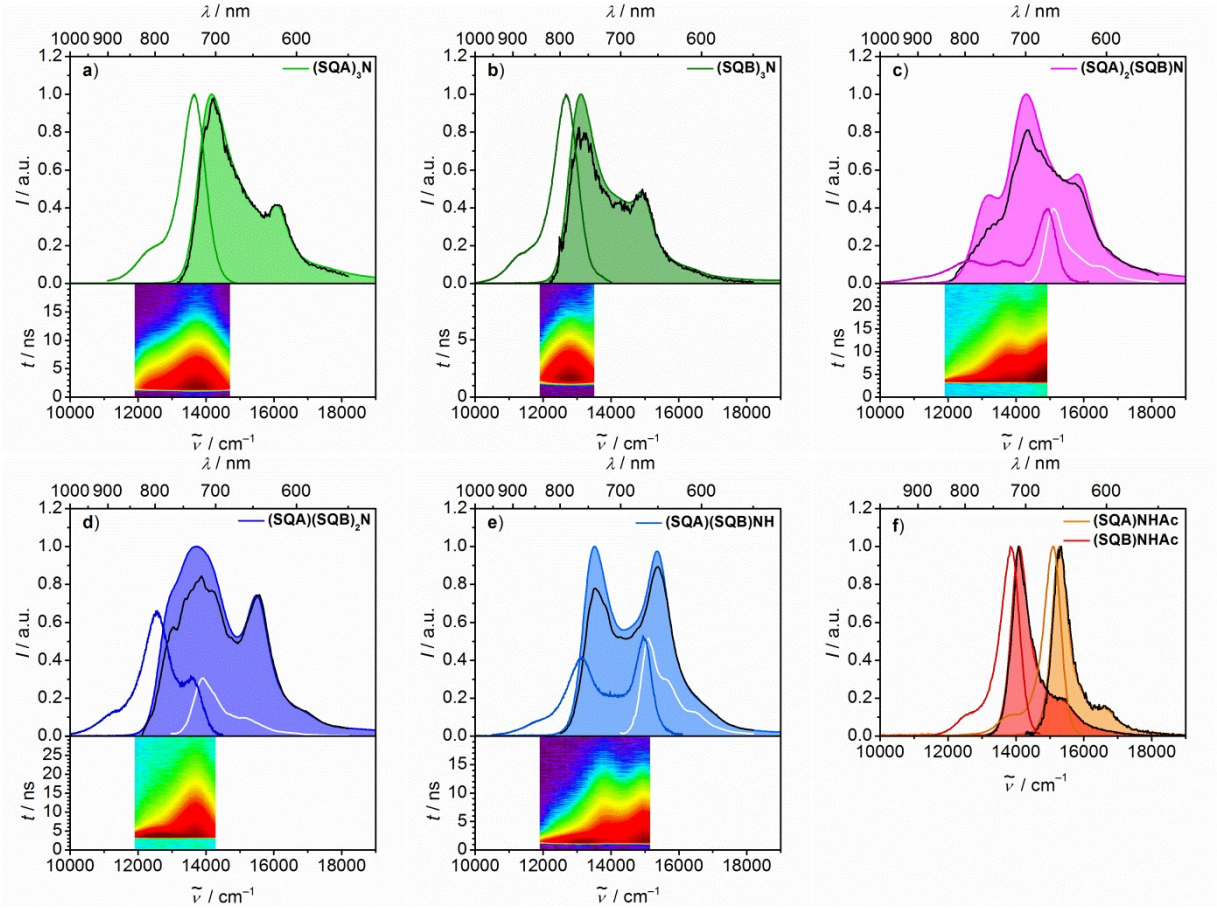

Fig. 4. Absorption spectra (shaded areas), fluorescence spectra (coloured solid lines), excitation spectra measured at low energy emission (black solid lines) and at high energy emission (solid white lines) of superchromophore squaraines and the monomers in toluene at RT. The fluorescence emission maps reflect intensity and decay dynamics for excitation at 15200 cm^{-1}. The excitation wavenumbers (ex) for the fluorescence spectra and the emission wavenumbers (em) for the excitation spectra were as follows: a) ex: 15200 cm^{-1}; em: 13300 cm^{-1} b) ex: 14300 cm^{-1}; em: 12700 cm^{-1} c) ex: 16700 cm^{-1}; em: 14900 cm^{-1}, 12700 cm^{-1} d) ex: 14900 cm^{-1}; em: 13700 cm^{-1}, 12300 cm^{-1} e) ex: 16700 cm^{-1}; em: 14900 cm^{-1}, 13000 cm^{-1} f) **(SQA)NHAc**: ex: 16100 cm^{-1}; em: 13900 cm^{-1}; **(SQB)NHAc**: ex: 15600 cm^{-1}; em: 12500 cm^{-1}.

measurements a combined deconvolution fit yielded, besides the isotropic decay time constants, the fluorescence anisotropy decay $r(t)$ and its initial amplitude. The latter gives information about relative orientation of transition moments and, thus, possible energy transfer processes. These measurements were performed exemplarily for one homotrimer **$(SQA)_3N$** and one heterotrimer **$(SQA)(SQB)_2N$** only. The isotropic decay is multiexponential in both cases (see Table 2) which suggests some structural reorganisation in the excited state. The initial anisotropy is quite small ($r(0)$ = 0.02 and 0.06) which indicates at least two-dimensional delocalisation of excitation (the theoretical values for parallel, perpendicular, 2D and 3D polarisation are 0.4, -0.2, 0.1 and 0) within the time-resolution of the measurement (IRF ca. 300 fs). The anisotropy decay constants are rather imprecise (1.5 ns for **$(SQA)_3N$** and 0.9 ns for **$(SQA)(SQB)_2N$**) because of the small amplitude but are on the order of diffusional rotation expected for the size of these superchromophores.[4, 27]

Our TA measurements have a much better time resolution (IRF ca. 140 fs), and allowed to excite the chromophores at various wavenumbers, that is, at the maximum of the lowest energy absorption and at the maximum of highest energy absorption of the exciton manifold (see Fig. 2). The excited states were probed by white light between 400-800 nm and in one case between 500-900 nm.

First, we describe and discuss the TA spectra of **$(SQA)_3N$** as an example. The transient maps of this chromophore upon excitation into the lowest exciton level (14200 cm^{-1}) show a strong ground state bleaching (GSB) signal around the steady state absorption of the chromophores merged with an also negative signal at the lower energy flank of the GSB caused by stimulated emission, SE, see Fig. 5a. This GSB/SE signal forms within instrument response time as an initially narrow negative peak at 14200 cm^{-1} which broadens within ca. 100 fs. This process has frequently been assigned to transient hole-burning of the ground state population.[28-34] However there is doubt whether this effect can really be discerned from coherent artefacts when pump and probe pulse overlap in time.[35] Therefore, we do not discuss this effect further. There is also a rather weak and unstructured excited state absorption (ESA) at wavenumber <18000 cm^{-1} (see Fig. 5a). A weak ESA is also found at around 15000-16000 cm^{-1} which is caused by excitation into a two-exciton state (see Fig. 2). These two-exciton states are formed by simultaneous excitation of

Table 2. Time-Resolved Optical Data of Squaraine Chromophores in Toluene at RT

	τ_f / ns (TCSPC)[a]	τ_i / ps (a_i) (FLUC)[b]	τ_a / ps ($r(t = 0)$) anisotropy (FLUC)[c]	τ / ps (TA)[d] excit. lowest exciton	τ / ps (TA)[d] excit. highest exciton
$(SQA)_3N$	0.08	4.2 (0.18)	1530 (0.03)		0.08
	0.13	67 (0.18)	[16100/13600]	3.6	4.9
	0.50	1020 (0.64)		240	190
	1.56	[16100/13600]		1400	1300
				[14200]	[16100]
$(SQB)_3N$	0.83				0.16
				7.3	10
				710	730
				[13200]	[14900]
$(SQA)(SQB)_2N$	0.07	16 (-0.10)	880 (0.06)	0.65	0.11
	0.30	350 (0.90)	[14400/11100]	20	6.7
	0.51	[14400/11100]		360	350
	3.22				770
				[13100]	[15500]
$(SQA)_2(SQB)N$	0.15				0.09
	0.29			1.3	
	1.74			17	7.2
	3.07			180	180
					1100
				[13200]	[15800]
(SQA)(SQB)NH	0.03				0.13
	0.05			1.4	
	0.33			8.4	5.7
	1.90			31	
				330	320
					2200
				[13500]	[15400]
(SQA)NHAc	0.40(0.04)				
	1.93(0.96)				
(SQB)NHAc	2.98				

[a] Global deconvolution of fluorescence spectra measured by TCSPC, excitation at 15200 cm^{-1}. The amplitude spectra can be found in the SI. For the monomers fluorescence was measured at the maximum only, amplitudes are given in brackets. [b] Isotropic fluorescence lifetime constants (amplitudes) measured by upconversion at the given [pump/fluorescence] wavenumbers. [c] Anisotropy lifetimes (initial amplitudes at $t = 0$) [pump/fluorescence] measured by FLUC. [d] Globally fitted lifetimes of SADS measured by TA [pump wavenumber].

two chromophore branches, a process which is forbidden from the ground state but allowed as consecutive processes in the TA experiment.[36-38] Their state energy can easily be estimated by adding the energies of the two individual excited states of the chromophore branches. All these signals decay multiexponentially (see Table 2) with only little shift/broadening of the principal GSB/SE signal. Quite similar behaviour is found for all other trimers and the dimer (see Fig. S1 to S5). The two-exciton state is however only visible as a reduced GSB at ca. 15000 cm^{-1} in the case of the dimer. In case of excitation into the highest exciton band at 16100 cm^{-1}, the TA spectra of **$(SQA)_3N$** show a somewhat modified behaviour. The GSB at ca. 16100 cm^{-1} is more pronounced and shows an initial rapid decay within ca. 100 fs (see time profile at 16200 cm^{-1} in Fig. 5d). This signal may be caused by diverse processes which are hard to discern given the short timescale: 1) A coherent artefact can be ruled out because excitation of **(SQA)(SQB)NH** at somewhat higher energy (16100 cm^{-1}) than the S_2-state (15400 cm^{-1}) yields the same signal contribution (see Fig. S6). 2) Preferred population of an exciton state in a mixture of conformers with slightly varying absorption spectra can be ruled out since a stiff squaraine dimer **pySQB** (Fig. 6) which cannot possess different conformers also shows this behaviour.[39] 3) Stimulated emission together with GSB from the higher exciton level. In this case, population transfer to the lower exciton states would go along with a decrease of the SE from the higher exciton state but the GSB caused by depopulation of the ground state would remain at the same spectral position irrespective which excited state is populated. With the same time constant of the population transfer to the lower exciton state, SE from the lower exciton state should increase. This is exactly what we observe. The expected increase of SE is visible in the time scan at ca. 14100 cm^{-1} as a smooth curvature around t = 0.3 ps. This becomes more apparent when comparing the time traces at 14100 cm^{-1} for both 14200 cm^{-1} and 16100 cm^{-1} excitation (see red shaded circle in Fig. 5). The signal around ca. 16100 cm^{-1} is further influenced by overlaid

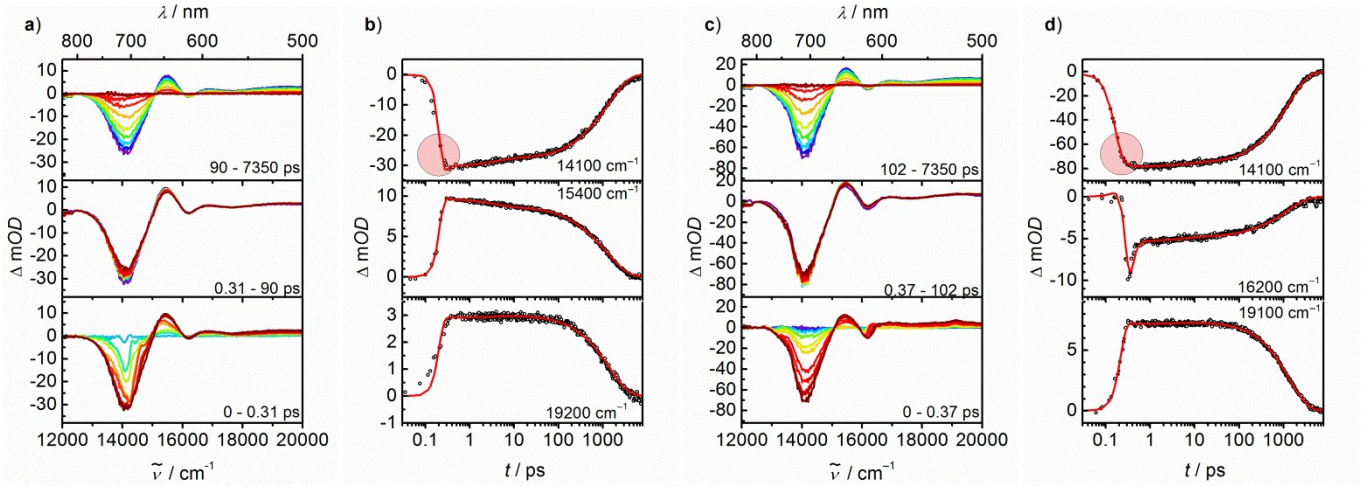

Fig. 5. Transient absorption spectra and time scans at selected wavenumbers of **(SQA)$_3$N** in toluene for excitation into the lowest exciton band at 14200 cm^{-1} (a, b) and the highest exciton band at 16100 cm^{-1} (c, d).

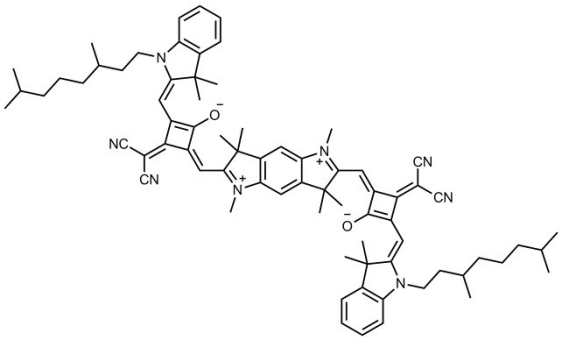

Fig. 6. Stiff squaraine dimer **pySQB**.

signal around ca. 16100 cm^{-1} is further influenced by overlaid ESA to the two-exciton states which increases in energy upon relaxation from the upper to the lower exciton state.

For a more detailed interpretation of the TA spectra we analysed the transient maps of all compounds for two different excitation wavenumbers globally using a heuristic target model given in Fig. 7 under the assumption that the ESA of all species associated difference spectra (SADS) have (almost) equal intensity at ca. 18000 cm^{-1}.[40] This requires in most cases that the efficiency for each particular step is adjusted as listed in Tables S1 to S10 in the SI. These SADS are given in Fig. 8. The discussion of the photoinduced processes is based on these SADS in the following.

In case of **(SQA)$_3$N** for the 14200 cm^{-1} excitation experiment three SADS (see Fig. 8a) were found whereby the short lifetime (3.6 ps) indicates fast vibrational relaxation or intramolecular vibrational energy redistribution[41-43] and the long lifetime (1.4 ns) is caused by ground state recovery. The intermediate lifetime (0.24 ns) is frequently observed in the relaxation of squaraine dyes[4, 24] and is probably associated with a slow structural reorganisation. The longer times are corroborated by the TCSPC measurements (0.13/0.50 and 1.56 ns). The TA experiment at 16100 cm^{-1} pump wavenumber gave four SADS (Fig. 8b): in addition to the two SADS also observed at lower pump wavenumber with similar lifetimes (4.9 ps and 0.19 ns) there is one component with a lifetime of 0.08 ps that shows an intense GSB at 16100 cm^{-1} and reduced SE at 13300-14300 cm^{-1} compared to the species with longer lifetime. This spectral component refers to what we tentatively interpret as the interband relaxation process mentioned above.

The other homotrimer **(SQB)$_3$N** behaves similarly to **(SQA)$_3$N** if excited at the lower exciton level. However, all spectral features are shifted to lower wavenumber and its lifetimes, in particular those associated with ground state recovery, are significantly shorter (see Fig. 8c). This may be a consequence of the energy gap rule. If excited at the highest exciton level, the homotrimer also shows an additional SADS (τ = 0.16 ps, see Table 2 and Fig. 8d), however with much less pronounced interband relaxation features at ca. 15000 cm^{-1}.

The heterotrimer **(SQA)$_2$(SQB)N** displays SADS being distinctly different from the homotrimers. For the excitation into the lowest exciton level at 13200 cm^{-1} three SADS can be discerned (Fig. 8e). All these SADS show two pronounced GSB signals at ca. 13000 cm^{-1} and 14200 cm^{-1}, a weaker one at 16100 cm^{-1} and an ESA around 15300 cm^{-1}. The latter two features are quite similar to those of the homotrimers. The two pronounced GSB signals refer to the two absorption peaks in the steady-state absorption spectrum at lower energy, the third peak at higher energy is reflected by the less intense GSB at 16100 cm^{-1}. From the difference of intensities of the SADS compared to the steady-state spectrum it is obvious that there must be a pronounced ESA into the two-exciton states overlaying the GSB signals. The three SADS possess lifetimes of 1.3 ps, 17 ps and 0.18 ns. The first two are associated with structural relaxation, the latter with ground state recovery. The fact that these three SADS show differences in band intensity at 13000 cm^{-1} and 15300 cm^{-1} must be caused by variation of SE and/or ESA because the GSB is expected to be the same for any delocalised excited state. This may easily be explained by slight changes of conformations between the

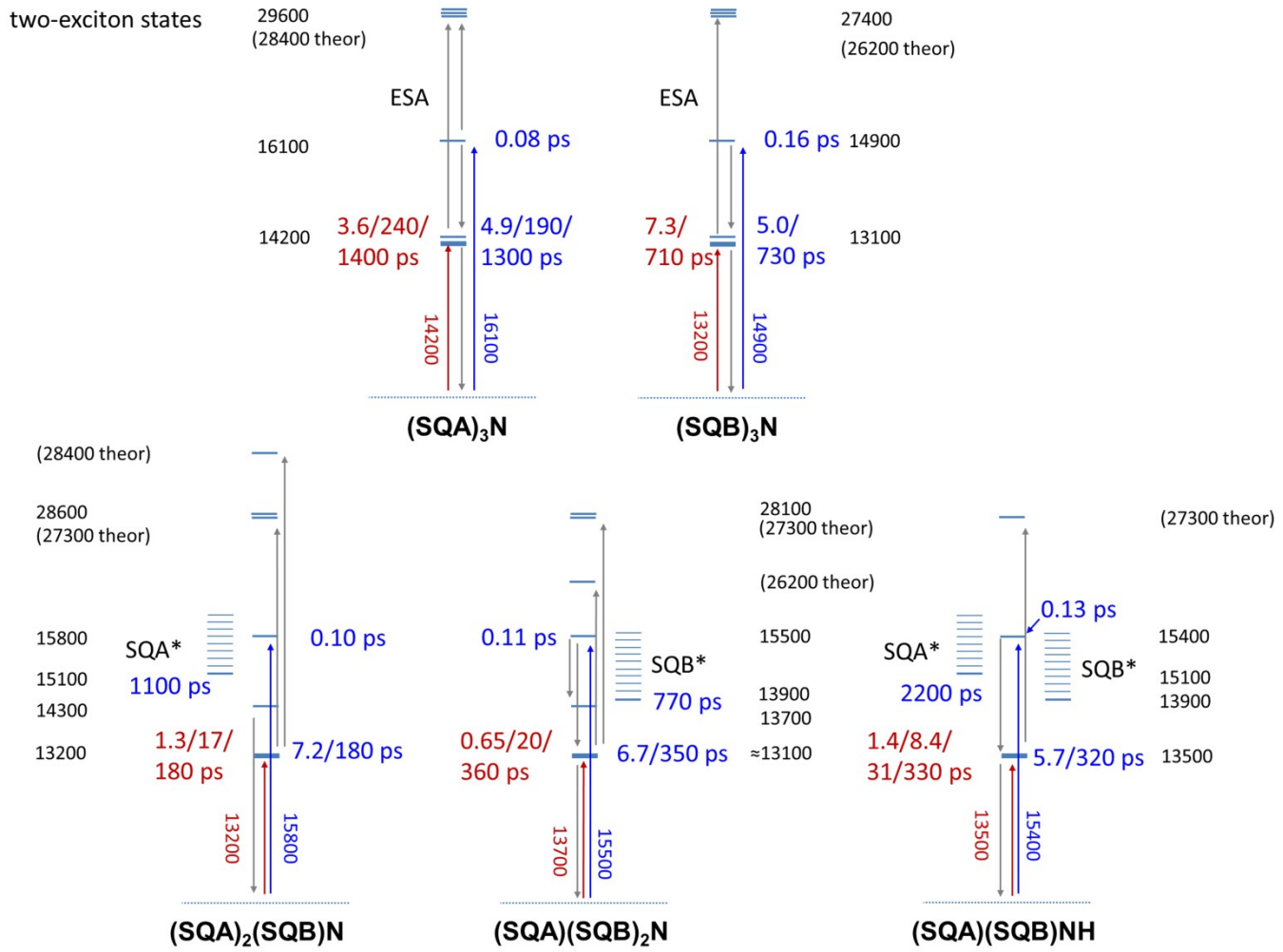

Fig. 7. State diagram used for the target analysis of the transient spectra. Lifetimes in red are for excitation into the lowest exciton band, those in blue for excitation into the highest exciton band at the given wavenumbers. The state energies were estimated by the peak positions of respective absorption bands, in case of the two-exciton states, they were estimated (= theor) from the respective energies in the homotrimers. The localised excited SQA* and SQB* states are given with their respective vibrational manifold to indicate spectral overlap with excitation at high energy. Lifetimes separated by a slash indicate multiexponential decay processes from multiple levels with slightly different energy (given as one bold bar). All the energy levels are not to scale.

three subchromophore branches which influence the oscillator strengths particularly strong due to variation of exciton coupling strength.

Excitation of **$(SQA)_2(SQB)N$** at 15800 cm^{-1} into the highest exciton state yields an SADS (Fig. 8f) with τ = 0.09 ps again with a strong negative signal around the excitation wavenumber which we interpret to be caused by GSB/SE of this exciton level. Accordingly, the peak at 13000 cm^{-1} of this SADS is smaller because of lack of SE. The other two SADS with τ = 7.2 ps and 0.18 ns are very similar to the corresponding ones of the 13200 cm^{-1} excitation experiment. However there is an additional SADS with τ = 1.1 ns with very low amplitude and which shows a totally different spectral form than the other SADS. From the steady-state and time-resolved emission spectra we have reasoned above that upon excitation of the highest exciton state, monomer-like states may be populated in parallel because the vibronic progression of these states extends to the excitation energy (see Fig. 7). Indeed, comparison of the SADS with τ = 1.1 ns with the combined absorption and emission spectrum of **(SQA)NHAc** (see Fig. S7) shows strong resemblance which supports the population of a localised SQA state in this case. Thus, we included this state in the target fit as a species excited in parallel whereby the initial population (ca. 10%, see Table S6) was adjusted to yield an SADS with comparable intensity as the other SADS.

For **$(SQA)(SQB)_2N$** the global fit of the TA map obtained by excitation into the lowest exciton state at 13100 cm^{-1} yields three SADS (Fig. 8g) with 0.65 ps, 20 ps and 0.36 ns. Excitation into the highest exciton band at 15500 cm^{-1} produces an additional SADS (Fig. 8h) with τ = 0.11 ps and a pronounced GSB/SE peak at 15600 cm^{-1} caused by the population of the upper exciton state. There is also an SADS with τ = 0.77 ns that looks like an SQB excited state as it resembles closely the spectral features (= sum of GSB and SE, see Fig. S8) of **(SQB)NHAc**. At this point we stress that the lifetime is associated with major uncertainties because of bad signal-to-noise ratio. In principal one would expect a lifetime in the lower ns time regime.

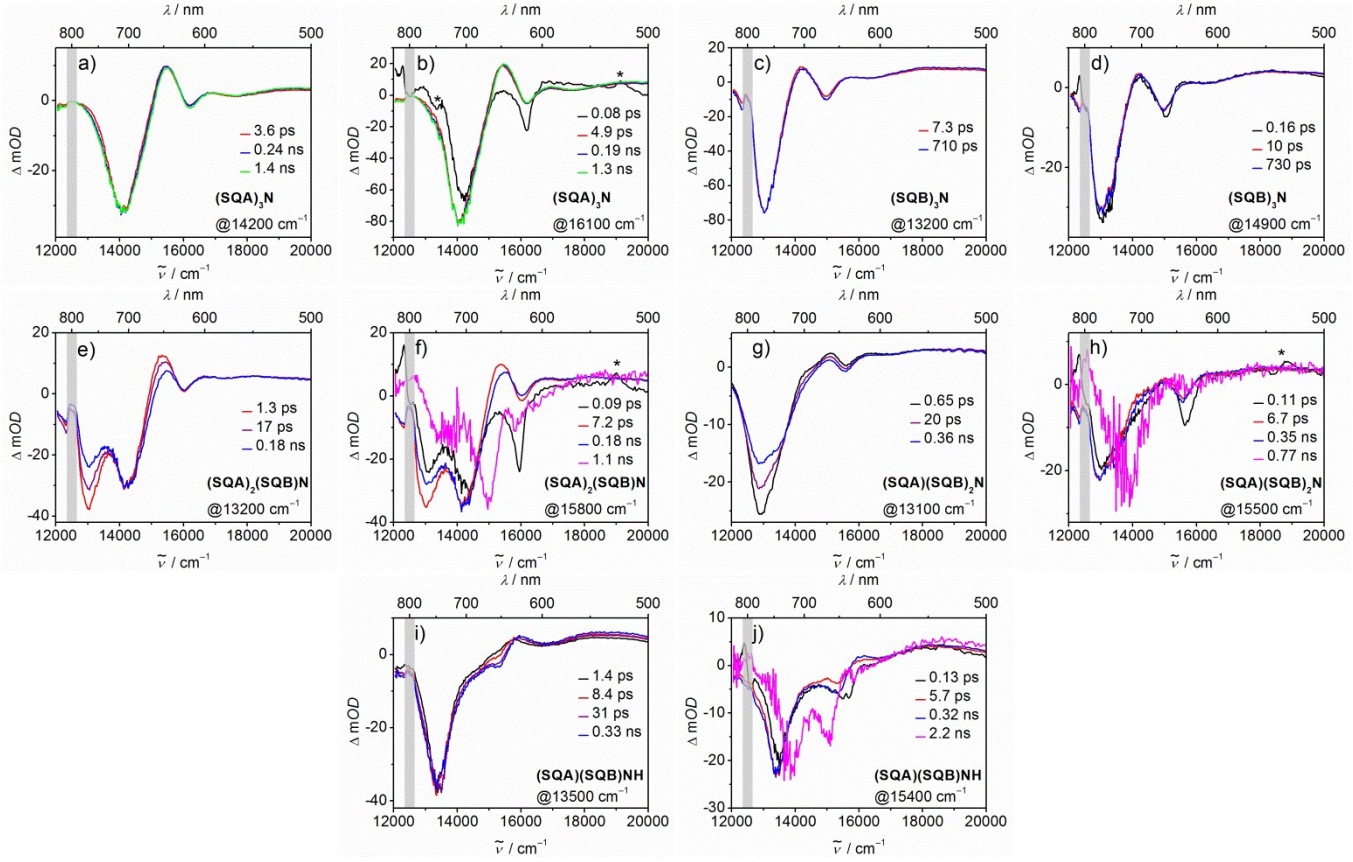

Fig. 8. Species associated difference spectra (SADS) for excitation into the lowest exciton state (a, c, e, g, i) and into the highest energy exciton state (b, d, f, h, j) of all homo and heterochromophores in toluene. The signals indicated with * are caused by the coherent artefact. The spectra at 800 nm ±10 nm (grey bar) are influenced by the laser fundamental and should be taken with caution. The colour code of the SADS refers to the dimension of lifetime with exception of the pink SADS which correspond to localised states.

In case of **(SQA)(SQB)NH** low energy excitation (13500 cm^{-1}) gives rise to four SADS with GSB/SE around 13400 cm^{-1} and little spectral changes around 15000 cm^{-1} (Fig. 8i). Again, the lifetimes span a range from 1.4 ps to 0.33 ns with the latter being the predominant lifetime for ground state recovery. At 15400 cm^{-1} excitation (Fig. 8j), an SADS with τ = 0.13 ps shows somewhat stronger GSB/SE at 15500 cm^{-1} and accordingly a lack of SE at the low energy side of the prominent negative signal around 13000 cm^{-1}. A fourth component with τ = 2.2 ns has two GSB maxima (13800 and 14900 cm^{-1}) each corresponding to the SQA and SQB state, respectively (see comparison with the respective GSB/SE spectra in the Fig. S9). Because of the low signal-to-noise ratio we observe a single lifetime (τ = 2.2 ns) for these two states.

DISCUSSION AND CONCLUSION

It appears that upon excitation of the highest exciton state in the hetero superchromophores localised squaraine states (SQA or SQB) are populated to a minor extent in parallel because their respective vibrational manifold leads to a significant absorption at the excitation energy. Such a population of a localised SQA or SQB states requires electronic decoupling from the rest of the molecule which is then left unexcited. The population of localised SQA or SQB states takes place exclusively in cases of the heterochromophores, that is, the SQA state in case of **$(SQA)_2(SQB)N$**, the SQB state in case of **$(SQA)(SQB)_2N$**, and both localised SQA and SQB states in case of the dimer **(SQA)(SQB)NH**. This behaviour can be rationalised easily as for e.g. **$(SQA)_2(SQB)N$** population of a localised SQA (= (SQA*)(SQA)(SQB)N) state leaves a fragment containing SQA and SQB in its ground state. The two chromophore branches in this (SQA)(SQB)N fragment could either be excited independently if they are electronically decoupled, or, if they are excitonically coupled, can be excited together. The first case can be ruled out as we would expect to see a localised SQB as well, which we do not. In the case of coupled SQA/SQB we would expect to see spectral components similar to the dimer **(SQA)(SQB)NH**. However, given the small amount of localised states formed (< 10%) these spectral features will easily hide among those of the excitonically coupled heterotrimer, as they are rather similar. And indeed we do not observe such specific dimer features. However, support for the latter interpretation comes from the analysis of the **(SQA)(SQB)NH** dimer spectra. Here we indeed see both localised SQA and SQB states because once one chromophore branch is electronically decoupled, the other one inevitably has also to be decoupled and both branches can then be excited separately.

This scenario leaves us with the question what the reason for the electronic decoupling is and why it does not take place in case of homotrimers. We may illustrate the electronic

situation for the heterodimer as an example. Here, simple exciton coupling theory tells us that the wavefunctions of the two exciton states are given by a linear combination of

$\Psi_+ = \sqrt{\frac{1+s}{2}}\psi_1 + \sqrt{\frac{1-s}{2}}\psi_1$ and $\Psi_- = \sqrt{\frac{1-s}{2}}\psi_1 - \sqrt{\frac{1+s}{2}}\psi_1$

where $s = 2\Delta E / \sqrt{4\Delta E^2 + 4J^2}$. If Δ*E* gets much larger than *J* the probability of finding the excitation on one chromophore branch ($\frac{1-s}{2}$) or the other ($\frac{1+s}{2}$) approaches either zero or unity. Thus, with increasing energy separation 2Δ*E* of the two monomer branches SQA and SQB the excitation becomes increasingly localised on one of these branches. We assume that small perturbations such as solvent fluctuations or thermal motions may induce a complete biasing of one of these branches.[44] In case of the homotrimers the probability of finding an excitation is equal (= 1/3) for each chromophore branch and fluctuations under the given conditions are not strong enough to perturb this situation in order to induce localisation of excitation. Another explanation may be based on different conformers. The orientation of chromophores in Fig. 1 is highly idealised. Given the fact that the central triphenylamine core adopts a propeller-like geometry, several conformers may result, where in some of those the orientation of two chromophores leads to a vanishing electronic exciton coupling. However in this case it is less obvious why this should not be the case for the homotrimers. This is why we favour the interpretation based on thermal motions/fluctuations.

In any case, the fact that the localised SQA or SQB state has a lifetime on the order of nanoseconds raises the question why no energy transfer takes place to lower lying states in the heterotrimers, thus shortening the lifetime of the localised states. Arguments based on Förster dipole-dipole energy transfer concerning distance of energy donor and acceptor as well as the spectral overlap issues cannot be raised as these criteria are certainly fulfilled and would allow fast energy transfer. However, unfavourable orientation of transition dipoles may indeed slow down energy transfer. A look at the estimated localised transition moments (Fig. 1) of the heterotrimers shows that those of one SQA and of one SQB are almost perpendicular which may reduce the dipole-dipole coupling considerably. As to what extent this reduced coupling can slow down energy transfer sufficiently is a matter of current debate as Langhals and Riedle[45] recently showed that even in cases of perfect perpendicular orientation of chromophores, vibronic coupling can induce very fast energy transfer.

Concerning the intraband relaxation within the exciton manifold, we interpret the GSB/SE signal around the excitation wavenumber observed upon excitation of the highest exciton state as an indication for the almost selective population of this state at this energy. The associated lifetime for all homo and heterochromophores is ca. 0.1 ps which is close to the resolution of our set-up. Therefore, we take these lifetimes as an upper bound of the real lifetime of the upper exciton state. Indeed, recent coherent optical 2D experiments with squaraine polymers gave intraband relaxations of a few 10 fs.[46]

The electronic coupling in the star-like trimers as evaluated in this work (ca. 600-700 cm^{-1}) is slightly larger than in the cyclic squaraine trimer (572 cm^{-1}) built from three SQB squaraine chromophores investigated recently.[3] Despite the different geometric arrangement which would favour emission from allowed states in the symmetric homotrimers, the fluorescence quantum yield is only 0.10 for **$(SQB)_3N$** while that of the cyclic trimer $c(SQB)_3$ is 0.14.[47] In the latter -although formally forbidden- symmetry breaking makes the lowest exciton states allowed transitions. This clearly shows that symmetry considerations may be disregarded when designing larger somewhat flexible chromophores for fluorescence application as symmetry breaking may override symmetry arguments and other effects may predominate in the fluorescence vs. nonradiative issues.

The main conclusion from this work is that combining two different squaraines in star-like arrangements brings about a broadening of absorption that surmounts that of analogous homotrimers. However, these heterosquaraine super-chromophores may populate localised states which counteract the delocalised states formed by exciton coupling. These local states may have a rather long lifetime which is not reduced by energy transfer to lower lying states. Thus, the strategy to broaden the absorption by using different chromophores that are coupled excitonically comes to an end if static disorder or dynamic fluctuations induce localisation of excitation.

EXPERIMENTAL

Steady-State Absorption Spectroscopy. All dyes were dissolved in toluene (Uvasol from Merck) and the UV/vis/NIR-absorption spectra were measured in 1 cm quartz cuvettes from Hellma using a Jasco V-670 spectrometer. The pure solvent was used as reference.

Femtosecond Transient Absorption Spectroscopy. The samples were dissolved in toluene (Uvasol from Merck), degassed for 30 min, filtered and stirred throughout the measurement. The experiments were performed in 2 mm fused silica cuvettes (Spectrocell Inc.) at RT and the optical density was adjusted to ca. 0.3 at the corresponding excitation wavenumber. The pump-probe measurements were performed with a Helios transient spectrometer from Ultrafast Systems and an amplified Ti:sapphire oscillator (Solstice) from Newport Spectra Physics (pulse length of 100 fs) with a repetition rate of 1 kHz and a fundamental wavenumber of 12500 cm^{-1} (800 nm). The output beam from the Solstice amplifier was split into two parts. A small part was focused onto a vertically oscillating CaF_2 crystal to generate a white light continuum between 11800 cm^{-1} (850 nm) and 28600 cm^{-1} (350 nm) which was polarised horizontally (the polarisation was adjusted by using a wire grid (Thorlabs)). The pulse was restricted with filters and used as the probe pulse. The main part was used to pump an optical parametric amplifier (TOPAS-C) from Light Conversion to generate the pump pulse with a pulse length of 140 fs at the corresponding excitation wavenumbers. By means of a wire grid (Moxtek) the

polarisation axis of the pump pulse was set to magic angle relative to that of the probe beam. The pump pulse (50 nJ, Ø ca. 0.1 mm) and probe pulse (Ø ca. 0.5 mm) met at ca. 6° vertical angle in the sample cuvette. The probe light was measured by a spectrograph equipped with a CMOS sensor (Ultrafast Systems, Helios) in the range between 11900 cm^{-1} (840 nm) and 25000 cm^{-1} (400 nm) with an intrinsic resolution of 1.5 nm. Every second pump pulse was blocked by a mechanical chopper (working at 500 Hz) to measure I and I_0. In order to compensate intensity fluctuations, a reference beam was split off and also detected with an identical spectrograph.

In order to cover the spectral range from 11000 cm^{-1} (910 nm) down to 22000 cm^{-1} (455 nm) accurately without interference around 12500±200 cm^{-1} (800±10 nm) with the fundamental, we used in one TA experiment a small portion of the light coming from the TOPAS (6500 cm^{-1} / 1530 nm) which was frequency doubled. The 13100 cm^{-1} (765 nm) and 6500 cm^{-1} (1530 nm) beams were separated. The 13100 cm^{-1} beam was used as the pump pulse and the 6500 cm^{-1} beam to generate white light in a CaF_2 crystal. Because of larger temporal white light fluctuation, the signal-to-noise ratio is much worse than in all other TA experiments. However, these TA spectra show the accurate spectral shape of GSB/SE band in the 11100-14300 cm^{-1} (900-700 nm) region.

By means of a computer-controlled linear stage (retro reflector in double pass setup) the relative temporal delay between pump and probe pulse was varied in 20 fs steps from 0 fs to 4 ps and from 4 ps to 8 ns in logarithmic steps with a maximum step size of 200 ps. Steady state absorption spectra were recorded before and after the transient absorption experiment to exclude degradation of the sample. The raw data were corrected for stray light prior to data analysis of the difference spectra map (time × wavelength).

The maps recorded under magic angle conditions were analysed with GLOTARAN[48, 49] including the correction for the white light dispersion (chirp) and modelling the instrument response function and the coherent artefact.

Emission Spectroscopy. Steady-state fluorescence measurements were performed with an Edinburgh Instruments FLS980 spectrometer. The compounds were dissolved in toluene (Uvasol from Merck) and purged with argon gas for 30 min prior to each measurement. Fluorescence quantum yields were measured with an integrating sphere and the FLS980 spectrometer applying the method of Bardeen et al.[50] to correct for self-absorption. Fluorescence lifetimes were determined by time-correlated single-photon counting (TCSPC) with the FLS980 spectrometer by exciting the samples with a pulsed laser diode at 15200 cm^{-1} (656 nm) under magic angle conditions and using a fast PMT detector (H10720) for fluorescence detection. Deconvolution of the data (4096 channels) was done by measuring the instrument response function with a scatterer (LUDOX).

Femtosecond Fluorescence-Upconversion Spectroscopy. We used a commercial fluorescence upconversion setup (Halcyone from Ultrafast Systems). The laser system was the same as for the fs-TA-experiments. The output beam was again divided in two parts. One part seeded the optical parametric amplifier (TOPAS-C from Newport Spectra Physics) to generate the pump pulse with a pulse length of 140 fs. The other part of the output beam was used as the gate pulse (12500 cm^{-1}, 800 nm) which was delayed over a maximum of 3 ns in 20 fs steps from 0 fs to 4 ps and in logarithmic steps from 4 ps to 3 ns with a maximum step size of 80 ps with a computer-controlled linear stage. The samples were prepared as for the fs-TA-experiments in 2 mm fused silica cuvettes (Spectrocell Inc.) and were stirred during the experiment. The pump pulse was focused onto the cuvette and the fluorescence light was collected and focused on a 0.5 mm BBO type II crystal for frequency upconversion with the gate. All lenses in the setup had a focal length of 100 mm and a thickness of 1.85 mm. The upconverted light was focused on the entrance slit of a double monochromator and measured by a PMT detector. For polarisation dependent measurements the pump beam was set to 45° by a $\lambda/2$ plate relative to the horizontally oriented gate beam. The polarisation of both beams was purified by wire grids (Moxtek). In front of the cuvette, the pump beam was finally adjusted to parallel, perpendicular and magic angle relative to the gate beam with a wire grid for reasons already explained in the section above. The anisotropic data were analysed by a simultaneous deconvolution fit of the parallel, perpendicular and magic angle traces at selected wavelengths with a self-written implementation in MatLab. A detailed description of this procedure can be found in literature.[51] Briefly, the measured signal intensity I is the convolution of the instrument response IRF (taken as Gaussian shaped) with the product of the population decay function S and respective anisotropy function which depends on r.

$$\begin{bmatrix} I_{\parallel}(t) \\ I_{\perp}(t) \\ I_{MA}(t) \end{bmatrix} = \left(S(t) \begin{bmatrix} 1+2r(t) \\ 1-r(t) \\ 1 \end{bmatrix} \right) \otimes IRF$$

Acknowledgements

We are indebted to Todd Marder for the opportunity to use his NIR fluorimeter. Furthermore, we thank the DFG for funding this work within the Research Group FOR 1809 and the Bavarian State Ministry for Education, Culture, Science, and the Arts (SolTech Initiative).

The authors declare no competing financial interest.

Notes and references

1. L. T. Dou, J. B. You, Z. R. Hong, Z. Xu, G. Li, R. A. Street and Y. Yang, *Adv. Mater.*, 2013, **25**, 6642-6671.
2. Y. W. Su, S. C. Lan and K. H. Wei, *Mater. Today*, 2012, **15**, 554-562.
3. C. Brüning, E. Welz, A. Heilos, V. Stehr, C. Walter, B. Engels, S. F. Völker, C. Lambert and V. Engel, *J. Phys. Chem. C*, 2015, **119**, 6174-6180.

4. C. Lambert, T. Scherpf, H. Ceymann, A. Schmiedel and M. Holzapfel, *J. Am. Chem. Soc.*, 2015, **137**, 3547-3557.
5. L. Beverina, R. Ruffo, G. Patriarca, F. De Angelis, D. Roberto, S. Righetto, R. Ugo and G. A. Pagani, *J. Mater. Chem.*, 2009, **19**, 8190-8197.
6. L. Beverina and P. Salice, *Eur. J. Org. Chem.*, 2010, 1207-1225.
7. P. Salice, J. Arnbjerg, B. W. Pedersen, R. Toftegaard, L. Beverina, G. A. Pagani and P. R. Ogilby, *J. Phys. Chem. A*, 2010, **114**, 2518-2525.
8. L. Beverina, R. Ruffo, M. M. Salamone, E. Ronchi, M. Binda, D. Natali and M. Sampietro, *J. Mater. Chem.*, 2012, **22**, 6704-6710.
9. L. Beverina and M. Sassi, *Synlett*, 2014, **25**, 477-490.
10. A. Ajayaghosh, *Chem. Soc. Rev.*, 2003, **32**, 181-191.
11. A. Ajayaghosh, *Accounts Chem. Res.*, 2005, **38**, 449-459.
12. S. Sreejith, P. Carol, P. Chithra and A. Ajayaghosh, *J. Mater. Chem.*, 2008, **18**, 264-274.
13. P. Anees, S. Sreejith and A. Ajayaghosh, *J. Am. Chem. Soc.*, 2014, **136**, 13233-13239.
14. L. Hu, Z. Q. Yan and H. Y. Xu, *RSC Adv.*, 2013, **3**, 7667-7676.
15. T. Geiger, S. Kuster, J. H. Yum, S. J. Moon, M. K. Nazeeruddin, M. Gratzel and F. Nuesch, *Adv. Funct. Mater.*, 2009, **19**, 2720-2727.
16. S. Kuster and T. Geiger, *Dyes Pigment.*, 2012, **95**, 657-670.
17. S. Kuster and T. Geiger, *Dyes Pigment.*, 2015, **113**, 110-116.
18. C. J. Qin, W. Y. Wong and L. Y. Han, *Chem.-Asian J.*, 2013, **8**, 1706-1719.
19. G. Chen, H. Sasabe, T. Igarashi, Z. R. Hong and J. Kido, *J. Mater. Chem. A*, 2015, **3**, 14517-14534.
20. T. A. Fayed, in *Reviews in Fluorescence 2009*, ed. C. D. Geddes, Springer, New York, 2011, vol. 2009, pp. 75-111.
21. S. F. Völker, T. Dellermann, H. Ceymann, M. Holzapfel and C. Lambert, *J. Polym. Sci. Pol. Chem.*, 2014, **52**, 890-911.
22. U. Mayerhöffer, M. Gsänger, M. Stolte, B. Fimmel and F. Würthner, *Chem.-Eur. J.*, 2013, **19**, 218-232.
23. M. Kasha, H. R. Rawls and M. A. El-Bayoumi, *Pure Appl. Chem.*, 1965, **11**, 371-392.
24. S. F. Völker, A. Schmiedel, M. Holzapfel, K. Renziehausen, V. Engel and C. Lambert, *J. Phys. Chem. C*, 2014, **118**, 17467-17482.
25. e.g. for **$(SQA)_2$(SQB)N**: 2 x 736 cm^{-1} + 630 cm^{-1}/3 = 700 cm^{-1}
26. W. W. Parson, in *Modern Optical Spectroscopy*, Springer, 2009, p. 293.
27. F. Zieschang, A. Schmiedel, M. Holzapfel, K. Ansorg, B. Engels and C. Lambert, *J. Phys. Chem. C*, 2013, **117**, 19816-19831.
28. K. Nishiyama and T. Okada, *J. Phys. Chem. A*, 1997, **101**, 5729-5735.
29. S. A. Kovalenko, J. Ruthmann and N. P. Ernsting, *J. Chem. Phys.*, 1998, **109**, 1894-1900.
30. M. D. Edington, R. E. Riter and W. F. Beck, *J. Phys. Chem. B*, 1997, **101**, 4473-4477.
31. K. Gibasiewicz, V. M. Ramesh, A. N. Melkozernov, S. Lin, N. W. Woodbury, R. E. Blankenship and A. N. Webber, *J. Phys. Chem. B*, 2001, **105**, 11498-11506.
32. H. Murakami, S. Kinoshita, Y. Hirata, T. Okada and N. Mataga, *J. Chem. Phys.*, 1992, **97**, 7881-7888.
33. P. Martinsson, J. A. I. Oksanen, M. Hilgendorff, P. H. Hynninen, V. Sundstrom and E. Akesson, *Chem. Phys. Lett.*, 1999, **309**, 386-394.
34. S. A. Kovalenko, N. P. Ernsting and J. Ruthmann, *J. Chem. Phys.*, 1997, **106**, 3504-3511.
35. T. J. Kang, J. W. Yu and M. Berg, *J. Chem. Phys.*, 1991, **94**, 2413-2424.
36. H. v. Amerongen, L. Valkunas and R. v. Grondelle, in *Photosynthetic Excitons*, World Scientific, Singapur, 2002, ch. 3, pp. 73-118.
37. J. Knoester, in *Proceedings of the International School of Physics "Enrico Fermi" Course CXLIX*, eds. V. M. Agranovich and G. C. La Rocca, IOS Press, Amsterdam, 2002, pp. 149-186.
38. In case of the heterotrimers, there are two sets of two-exciton states because there are two different combination of the two different chromophore branches, like and unlike.
39. C. Lambert, A. Schmiedel, M. Holzapfel, M. Schreck, L. Wittmann, unpublished results.
40. The shortest component (τ < 1 ps) was not adjusted as this would in most cases require direct ground state recovery which is unlikely at this short time scale.
41. M. Glasbeek and H. Zhang, *Chem. Rev.*, 2004, **104**, 1929-1954.
42. T. Elsaesser and W. Kaiser, *Annu. Rev. Phys. Chem.*, 1991, **42**, 83-107.
43. A. Pigliucci, G. Duvanel, L. M. L. Daku and E. Vauthey, *J. Phys. Chem. A*, 2007, **111**, 6135-6145.
44. J. Arago and A. Troisi, *Phys. Rev. Lett.*, 2015, **114**.
45. H. Langhals, A. J. Esterbauer, A. Walter, E. Riedle and I. Pugliesi, *J. Am. Chem. Soc.*, 2010, **132**, 16777-16782.
46. C. Lambert, F. Koch, S. F. Völker, A. Schmiedel, M. Holzapfel, A. Humeniuk, M. I. S. Rohr, R. Mitric and T. Brixner, *J. Am. Chem. Soc.*, 2015, **137**, 7851-7861.
47. The quantum yield was corrected from a relative quantum yield measurement with the factor 1.25 to be comparable with the absolute quantum yield measurements employed in this work.
48. I. H. M. van Stokkum, D. S. Larsen and R. van Grondelle, *Biochim. Biophys. Acta-Bioenerg.*, 2004, **1658**, 262-262.
49. J. J. Snellenburg, S. P. Laptenok, R. Seger, K. M. Mullen and I. H. M. van Stokkum, *J. Stat. Softw.*, 2012, **49**, 1-22.
50. T. S. Ahn, R. O. Al-Kaysi, A. M. Mueller, K. M. Wentz and C. J. Bardeen, *Rev. Sci. Instrum.*, 2007, **78**.
51. M. Steeger, Ph.D. Thesis, University of Würzburg, 2015.